



**HAL**  
open science

# The El Asnam 1980 October 10 inland earthquake: a new hypothesis of tsunami generation

J. Roger, H. Hébert, J. -C. Ruegg, P. Briole

► **To cite this version:**

J. Roger, H. Hébert, J. -C. Ruegg, P. Briole. The El Asnam 1980 October 10 inland earthquake: a new hypothesis of tsunami generation. *Geophysical Journal International*, 2011, 185, pp.1135-1146. 10.1111/j.1365-246X.2011.05003.x . insu-03606473

**HAL Id: insu-03606473**

**<https://insu.hal.science/insu-03606473>**

Submitted on 12 Mar 2022

**HAL** is a multi-disciplinary open access archive for the deposit and dissemination of scientific research documents, whether they are published or not. The documents may come from teaching and research institutions in France or abroad, or from public or private research centers.

L'archive ouverte pluridisciplinaire **HAL**, est destinée au dépôt et à la diffusion de documents scientifiques de niveau recherche, publiés ou non, émanant des établissements d'enseignement et de recherche français ou étrangers, des laboratoires publics ou privés.



Distributed under a Creative Commons Attribution 4.0 International License

# The El Asnam 1980 October 10 inland earthquake: a new hypothesis of tsunami generation

J. Roger,<sup>1,2</sup> H. Hébert,<sup>2</sup> J.-C. Ruegg<sup>3</sup> and P. Briole<sup>1</sup>

<sup>1</sup>*Ecole Normale Supérieure, Laboratoire de Géologie, UMR 8538, 24, rue Lhomond, 75231 Paris, CEDEX 5, France. E-mail: jeanrog@hotmail.fr*

<sup>2</sup>*CEA, DAM, DIF, F-91297 Arpaçon, France*

<sup>3</sup>*Institut de Physique du Globe de Paris, laboratoire de Sismologie, 4 place Jussieu, 75252 Paris, CEDEX 5, France*

Accepted 2011 February 25. Received 2011 February 25; in original form 2010 August 5

## SUMMARY

The Western Mediterranean Sea is not considered as a high seismic region. Only several earthquakes with magnitude above five occur each year and only a handful have consequences on human beings and infrastructure.

The El Asnam (Algeria) earthquake of 1980 October 10 with an estimated magnitude  $M_s = 7.3$  is one of the most destructive earthquakes recorded in northern Africa and more largely in the Western Mediterranean Basin. Although it is located inland, it is known to have been followed by a small tsunami recorded on several tide gauges along the southeastern Spanish Coast. In 1954, a similar earthquake having occurred at the same location induced a turbidity current associated to a submarine landslide, which is widely known to have cut submarine phone cables far from the coast. This event was followed by a small tsunami attributed to the landslide. Thus the origin of the tsunami of 1980 was promptly attributed to the same kind of submarine slide. As no evidence of such mass movement was highlighted, and because the tsunami wave periods does not match with a landslide origin in both cases (1954 and 1980), this study considers two rupture scenarios, that the coseismic deformation itself (of about 10 cm off the Algerian coast near Ténès) is sufficient to produce a low amplitude (several centimetres) tsunami able to reach the Spanish southeastern coast from Alicante to Algeciras (Gibraltar strait to the west).

After a discussion concerning the proposed rupture scenarios and their respective parameters, numerical tsunami modelling is performed on a set of bathymetric grids. Then the results of wave propagation and amplification (maximum wave height maps) are discussed, with a special attention to Alicante (Spain) Harbour where the location of two historical tide gauges allows the comparison between synthetic mareograms and historical records showing sufficient signal amplitude.

This study is part of the active tsunami hazard assessment in Mediterranean Sea especially concerning its occidental part, that is, the Algerian, Spanish and French coasts.

**Keywords:** Tsunamis; Seismicity and tectonics; Continental margins: convergent; Fractures and faults; Africa; Europe.

## 1 INTRODUCTION

### 1.1 Generalities

Although the Western Mediterranean Sea does not have such active margins as the Eastern Mediterranean Sea (subduction under southern Italy and Greece), it is subject to low to moderate seismicity ( $M_w < 7.3$ ) mainly located in northern Africa, along the Algerian Margin and in the Alboran Sea. There is no general trend concerning the rupture mechanisms along this margin as it goes from pure compressive movement at the east (northern Italy/Tunisia/Algeria) to a pure strike-slip trend in Alboran Sea to the west.

We present a study of the tsunami associated with the 1980 October 10 El Asnam earthquake ( $M_s = 7.3$ ), which is the largest shallow event in the Western Mediterranean area during the 20th century. The epicentre has been estimated 45 km to the south of the Algerian shores of the Mediterranean Sea (Solovyev *et al.* 1992) in the same region of the 1954 Orléansville (renamed afterwards El Asnam) earthquake ( $M_s = 6.7$ , Rothé 1955). It is historically known that these two earthquakes have been followed by some sea level variations recorded on tide gauges located along the Spanish southeastern coast from Alicante to Algeciras (Gibraltar Strait). There are at least six tide gauge records available concerning the 1980 event. The tsunami was supposed to be generated by a

submarine turbidity current in both 1980 and 1954. The originality of this paper is that we propose that the tsunami may have been directly induced by the coseismic deformation of the earthquake without the need of submarine slide (not revealed yet by bathymetric surveys) as currently assumed for the 1980 event.

With the help of the numerous studies led after the earthquake (due particularly to the fact that this earthquake is associated with important vertical and horizontal movements) we propose a source composed of one or three segments and their associated parameters is able to generate a tsunami which can be recorded on Spanish coastal tide gauges and be compared to historical data.

## 1.2 Historical settings

### 1.2.1 The earthquake

On 1980 October 10 at 12h25 UTC, a magnitude  $M_s = 7.3$  earthquake occurred at El Asnam (actual Ech Cheliff) at  $36.159^\circ\text{N}$  and  $1.396^\circ\text{E}$  (USGS location – Dewey 1990; Fig. 1), causing thousands of casualties (Ambraseys 1981) and accompanied by an important coseismic deformation (Ruegg *et al.* 1982; Lammali *et al.* 1997). It is the largest instrumentally recorded earthquake in northern Africa (Cisternas *et al.* 1982). This event occurred nearly at the same location as the earthquake of 1954 (epicentre located at  $36.285^\circ\text{N}$ – $1.566^\circ\text{E}$ , i.e. in the locality of Beni-Rached) and is supposed to correspond to the release of accumulated strain either on the same fault segment or on two nearby distinct ones (Dewey 1990; Lammali *et al.* 1997).

On 1928 August 24 and 1934 September 7, two other less important fault ruptures ( $m_b = 5.4$  and  $5.0$ , respectively) occurred

on the same fault system of the 1954 and 1980 events; their epicentres have been located in Oued Rhiou, westward from El Asnam, and El Abadia, eastward of Beni-Rached (Fig. 1; Shah & Bertero 1980).

### 1.2.2 The tsunami

The two earthquakes of 1954 and 1980 were both followed by low amplitude tsunamis that reached the Spanish coast and were recorded by sea-level gauges located in some harbours (Solovyev *et al.* 1992). The event of 1980 has been recorded on six tide gauges located at Alicante (one on the outer breakwater and one on the inner breakwater), Cartagena, Almeria, Malaga and Algeciras (see locations on Fig. 1). Both in 1954 and in 1980, the best signal with the highest amplitude has been recorded on the Alicante instruments. Nevertheless there is no strong difference between the signal recorded at Algeciras, that is, the furthest in the Alboran Sea, and the signal recorded in Almeria in terms of maximum wave amplitude and period. The recorded signals with their respective frequency spectra are shown in Fig. 2. Arrival times identified by Solovyev *et al.* (1992) are also indicated: they are in good agreement with the theoretical tsunami traveltime (TTT) calculation shown on Fig. 2. The record in Cartagena has not been published because of its poor quality (Solovyev *et al.* 1992). Only three gauges have recorded both signals: Alicante (outer gauge), Malaga and Algeciras; at the three locations the maximum wave heights are reached for the 1954 event with a factor of 2 between 1954 and 1980.

It is generally accepted that the tsunami observed in 1980 was related to turbidity currents (Solovyev *et al.* 1992, 2000;

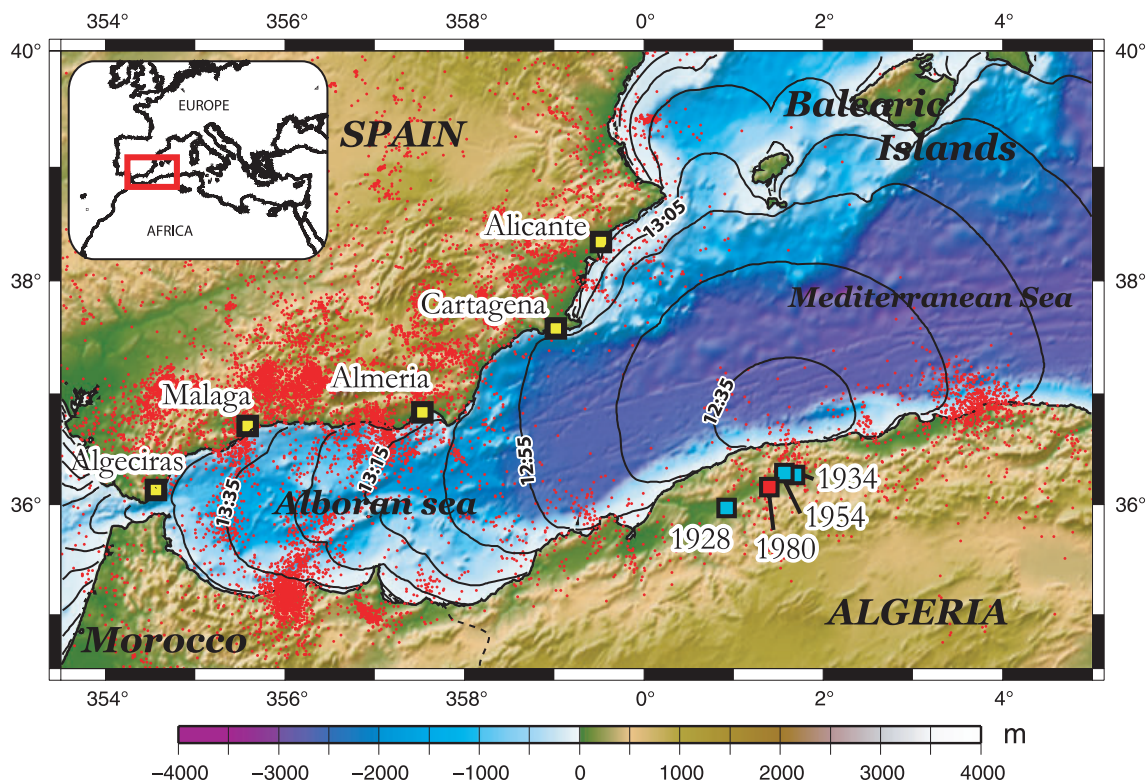
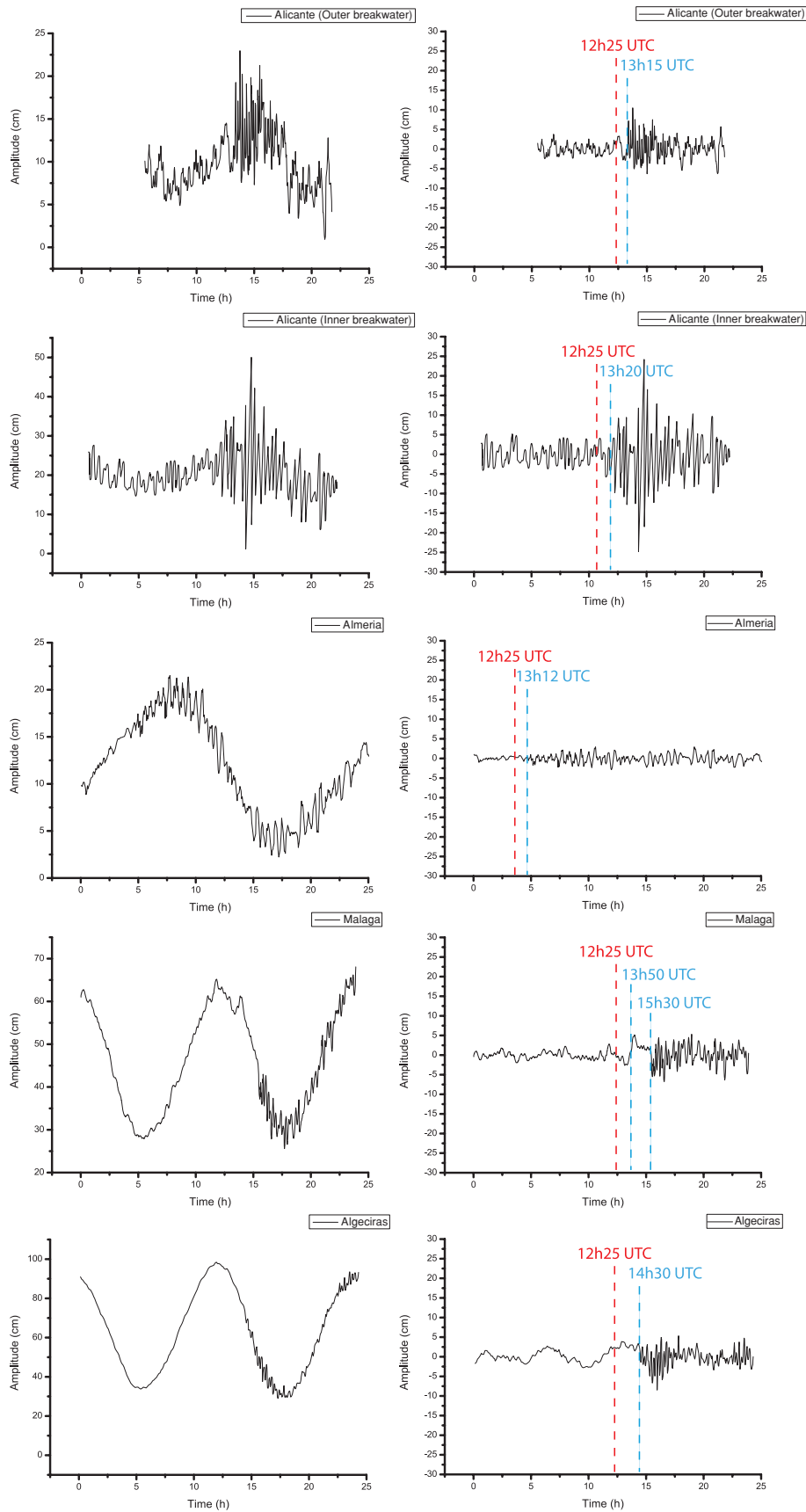


**Figure 1.** Location of the epicentres of the El Asnam earthquake of 1980 October 10, the 1954 Orléansville earthquake and the 1928 and 1934 events. The six tide gauges (two at Alicante) that recorded the tsunami are also indicated by yellow-black boxes. The red dots represent the local seismicity (data USGS, from 1973 to present). The black solid curves represent the theoretical tsunami traveltimes for a source located offshore El Asnam area and computed using the TTT SDK v 3.2 (<http://www.geoware-online.com>).



Downloaded from https://academic.oup.com/gji/article/185/3/1135/601483 by guest on 12 March 2022

**Figure 2.** Historical tide gauge records at the locations indicated on Fig. 1: original (left-hand panels) and residual (detided) (right-hand panels). The time of the earthquake is pointed in red and the tsunami arrival as pointed in blue as indicated by Solovyev *et al.* (1992).

Papadopoulos *et al.* 2007), which have been reported for several earthquakes along the north Algerian Margin. The reason is found during the 1954 earthquake, when some submarine phone cables (five of the eight actives at that time exactly) offshore of Algeria were seriously damaged (as far as 100 km from the coast): this phenomenon has been associated with the motion of one or several turbidity currents generated by seismic shaking and/or submarine landslides (Heezen & Ewing 1955; Bourcart & Glangeaud 1956; Solovyev *et al.* 1992). Events where damage has occurred to three of these cables are described in Heezen & Ewing (1955): the first cable, located less than 40 km from the shore, ruptured 40 min after the earthquake; the last one, located 110 km from the Algerian shore, ruptured 5 hr after the earthquake. This is in opposition to the fast recorded TTT of about 50 min for Alicante Harbour, 250 km away from the Ténès shore. In addition, it is reported that those cables were dashed-damaged, that is, that some segments were damaged and others not, revealing several different turbidity currents and/or landslides. Concerning the 1980 event, there were fewer cables in activity near the Algerian Margin than in 1954 and only one cable rupture, linked to a small turbidity current near the bay of Algiers (200 km from epicentre), has been reported (El-Robrini *et al.* 1985). According to the recent marine surveys on the Algerian Margin, no recent scarp and/or important mass transport deposits have been highlighted offshore of the Ténès region (Cattaneo *et al.* 2010). In addition, Bourcart & Glangeaud (1956) indicate that a single turbidity current generated by the main shock in 1954 is not able to explain, alone, the rupture of all cables, some of them were located too far away from the slide location; some secondary slides generated by aftershocks may have generated turbidity currents too.

Nevertheless, the destabilization of the sedimentary cover on the continental slope of the Algerian margin spawning turbidity currents is currently associated with strong earthquakes (Yelles Chaouche 1991; Cattaneo *et al.* 2010).

If related to any submarine landslide, the signal recorded along the Spanish coast requires an adequate period of several minutes, typically around 2–10 min at most (Kulikov *et al.* 1996; Assier-Rzadkiewicz *et al.* 2000; Ioualalen *et al.* 2010). Thus the measured period of the oscillations of about 15–25 min for both 1954 and 1980 events on each available record (Solovyev *et al.* 1992) are not consistent with a landslide source.

In addition it requires a very important submarine mass movement to produce some sea level disturbances of still several centimetres as distant as in the harbour of Algeciras (Fig. 2) located 500 km away from the source area (see location on Fig. 1). In fact the reason is that since short tsunami wavelengths related to a small extent of the source (typically landslide sources) are dispersed during the propagation, they are unable to retain their energetic content at distances. Even if several turbidity currents have been reported, they should have simultaneously occurred to produce sufficient tsunami amplitude. However, such coherent submarine landslides have not been highlighted during recent Maradja bathymetric and seismic studies (Domzig *et al.* 2009).

Correlated to the previous point, tsunamis generated by submarine landslides often exhibit very large, or at least significant, run-up heights close to the source area (Tappin *et al.* 2001; Okal & Synolakis 2004; Harbitz *et al.* 2006; Tappin *et al.* 2008), an occurrence not mentioned by eyewitnesses to the 1980 earthquake along the Algerian coast.

These considerations allow us to propose a pure earthquake origin for the 1954 and 1980 tsunamis. In the following, we provide additional constraints from numerical modelling that confirm this hypothesis.

## 2 NUMERICAL MODELLING

### 2.1 Sources parameters

The detailed analysis of the El Asnam 1980 earthquake reveals a predominant thrusting mechanism on a fault plane split into three main segments (Fig. 3)—called southwestern, central and north-eastern in the following—(Yielding *et al.* 1981; King & Yielding 1984), linked to each other by some smaller segments, with an average strike N45°E and with a mean dip angle of 54° to the north-west (Ambraseys 1981; Cisternas *et al.* 1982; Deschamps *et al.* 1982) combined with a small left-lateral displacement (Philip & Meghraoui 1983; Solovyev *et al.* 1992) which is apparently not significant (Nabelek 1985). This mechanism is well revealed by the field analysis that shows an important uplift of several metres all along the surface rupture, with a maximum of about 5–6 m in the area located northwest of the junction of the southern and central fault segments associated with a depression of about 1 m southeast of it (Kasser *et al.* 1987; Ruegg *et al.* 1982; Shah & Bertero 1980). This overall rupture pattern is directly related to the compressional regional setting associated with the active convergence between the European and African plates (Ouyed *et al.* 1981; Boudiaf *et al.* 1998).

The magnitude of the El Asnam earthquake has been estimated as  $M_s = 7.3$  from surface waves (Cisternas *et al.* 1982; Deschamps *et al.* 1982). The energy magnitude is estimated to  $M_w = 7.1$  by the Global Centroid-Moment-Tensor (CMT) Project (<http://www.globalcmt.org/cgi-bin/globalcmt-cgi-bin/CMT4/>), with a seismic moment of about  $M_0 = 5.07 \times 10^{19}$  N-m. Because the well-accepted relationship between  $M_w$  and  $M_s$  allows us to estimate that  $M_w \approx M_s$  in the range of magnitude 5.5–7.5 (Hanks & Kanamori 1979; Wells & Coppersmith 1994), and because the energy magnitude released during the main shock is not constrained very well due to the lack of nearby stations at the time of the earthquake (the first stations were deployed only two days after the main shock), we decided to propose scenarios for a  $M_w = 7.3$  earthquake.

According to Wells & Coppersmith (1994), the surface and sub-surface rupture lengths are not necessarily different: they indicate that the ratio between those lengths could be equal to 1 for a  $M_w = 7.3$  earthquake. In addition, rupture plan length and width must be in a ratio of about 1:3.

Geodetic measurements help to partially constrain the average slip and the rake angle on the different fault plane (Ruegg *et al.* 1982; Yielding 1985; Bezzeghoud *et al.* 1995). We look at the geodetic measurements to choose the fault parameters with respect to the geological post-seismic surveys.

The rigidity coefficient  $\mu$  has been chosen assuming a standard rigidity of  $3.0 \times 10^{10}$  N m<sup>2</sup> (compression mechanism) in agreement with Bilek & Lay (1999) and Geist & Bilek (2001) for conventional earthquakes.

The dip angle is obtained with regard to the aftershock depth distribution (for example Yielding *et al.* 1989).

These analyses allow the proposal of several rupture scenarios. Only two will be presented in the following.

### 2.2 Rupture models

#### 2.2.1 First model: one-segment rupture

In order to simplify the problem we have considered for our calculation models that the rupture zone was made of only one fault plane (Fig. 3) encompassing the three identified segments (presented by

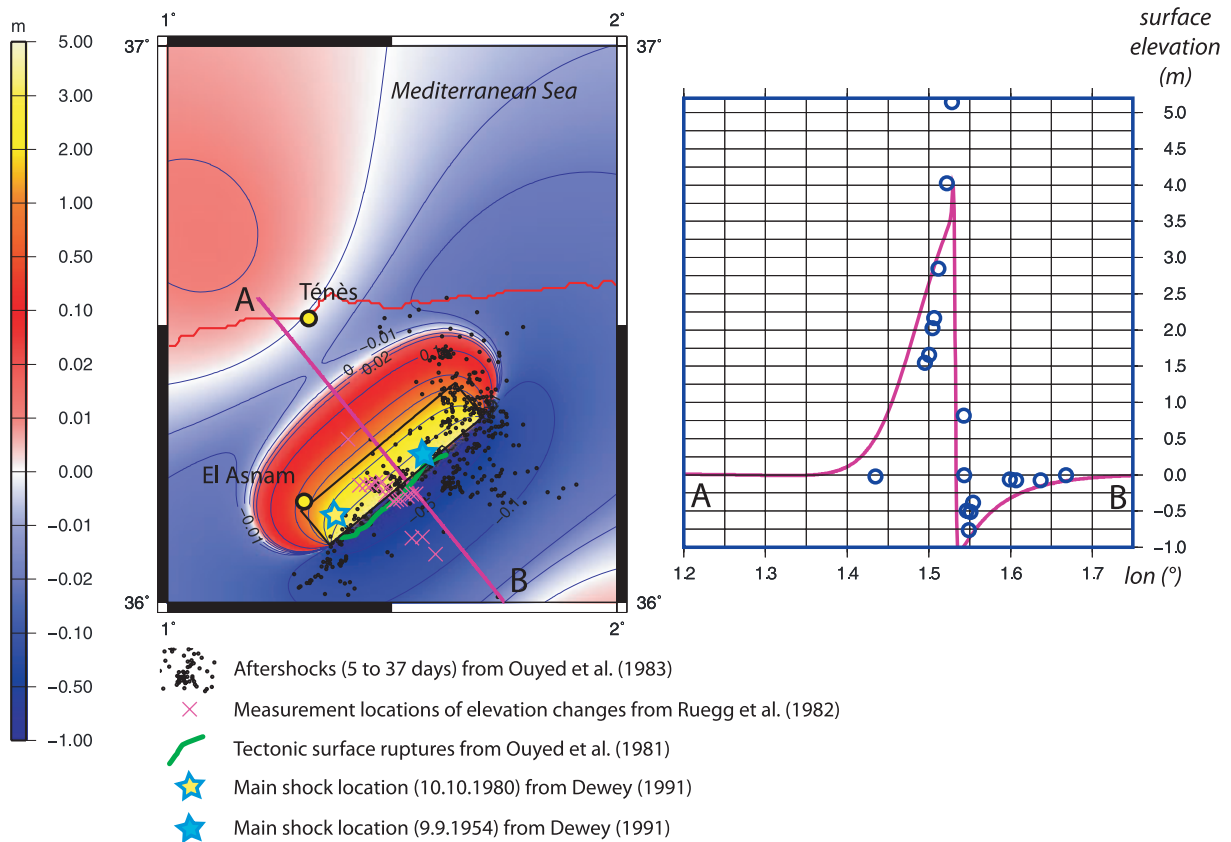


**Figure 3.** Coseismic deformation for a model composed of a single fault plane (black rectangle) corresponding to a  $M_w$  7.3 earthquake in the area of El Asnam. The locations of the surface breaks, main shocks of 1954 and 1980, and aftershocks’ epicentre from Ouyed *et al.* (1983) are indicated. A cross-section (A–B) in the middle of the rupture zone showing surface vertical displacement is represented (purple curve) and superimposed to on-field post-seismic measurements of elevation changes projected on a profile from Ruegg *et al.* (1982) (blue dots).

**Table 1.** Parameters for the two different scenarios of  $M_w = 7.3$  rupture for the 1980 earthquake discussed in this study.

	Longitude of fault plane centre (°)	Latitude of fault plane centre (°)	Depth of fault plane centre (km)	Coseismic slip (m)	Strike (°)	Dip (°)	Rake (°)	Length (km)	Width (km)	Rigidity ( $N\ m^{-2}$ )	Mo (N m)
1 segment	1.5	36.25	6.250	6	230	54	90	36	15	$30.10^9$	$1.1 \cdot 10^{20}$
3 segments	1.415	36.18	6.5	5	228	54	90	12	15	$30.10^9$	$1.1 \cdot 10^{20}$
	1.52	36.255	6.5	8	225	54	90	12	15	$30.10^9$	
	1.64	36.37	5.75	5	252	30	90	12	23	$30.10^9$	

Yielding *et al.* 1989, for example), assuming that the strike is nearly the same for each segment (Roger & Hébert 2008a). In this case of a unique fault plane, according to King & Vita-Finzi (1981) and Cisternas *et al.* (1982), a slip area of 40 km long and 15 km deep with a mean displacement of 6 m leads to an earthquake magnitude of  $M_w = 7.3$  (i.e.  $M_0 = 1.1 \times 10^{20}$ ). We will find the same orders for the parameters attributed to the multiple segments sources in the following (Table 1).

We will see further that this approach is rapidly limited since not enough deformation, according to the geodetic surveys (Yielding *et al.* 1981; Ruegg *et al.* 1982; Bezzeghoud *et al.* 1995), was then modelled in the central part of the segment. In fact, this single segment does not allow playing with the different parameters to best fit the observed data.

The advantage of using a multi-segments source is the possibility to vary the parameters of the part of the fault close to the sea, especially the slip value. The next subsection will debate the tsunami generation by both scenarios: such a unique fault plane is not able to

generate enough sea deformation to match the Spanish tide gauge signals and to amplify in the same height range of the historical data.

### 2.2.2 Second model: three-segment rupture

After a more detailed study of the literature on this event, a source composed of three distinct segments has been tested (Roger *et al.* 2009; Fig. 4). Their locations have been based on the aftershocks’ geographical location (Deschamps *et al.* 1982; Ouyed *et al.* 1983; King & Yielding 1984; Yielding *et al.* 1989; Bezzeghoud *et al.* 1995) and their depth distribution (Cisternas *et al.* 1982; Ouyed *et al.* 1983; Yielding *et al.* 1989).

The aftershocks’ studies (Ouyed *et al.* 1983; King & Yielding 1984; Yielding 1985; Yielding *et al.* 1989) show that they are mostly located near the rupture surface features in terms of horizontal distribution along the two southern segments. However, there is a widespread location of aftershocks toward the sea when we look

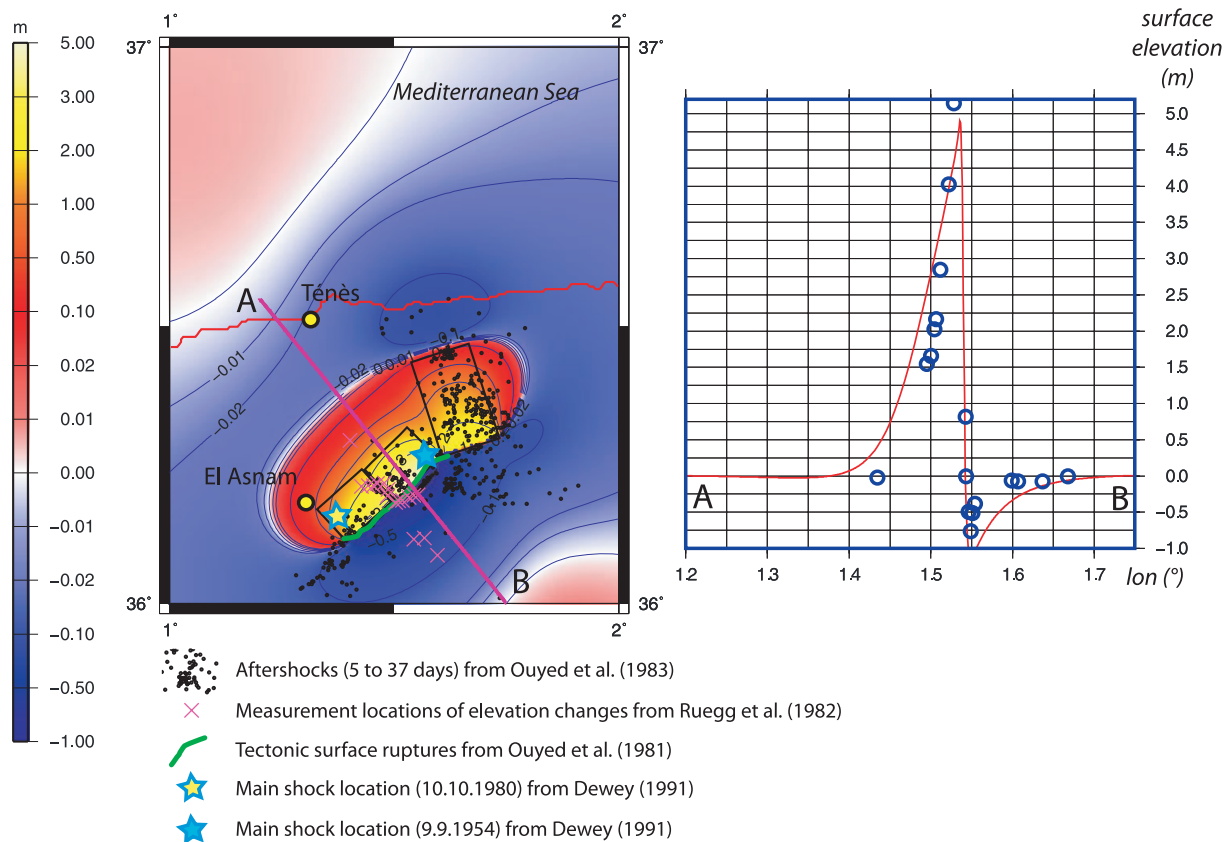


**Figure 4.** Coseismic deformation for a model composed of three fault segments matching the surface rupture segments exposed in the literature. The locations of the main shocks of 1954 and 1980, and aftershocks' epicentre from Ouyed *et al.* (1983) are indicated. A cross-section (A–B) in the middle of the rupture zone showing surface vertical displacement is represented (red curve) and superimposed to on-field post-seismic measurements of elevation changes projected on a profile from Ruegg *et al.* (1982) (blue dots).

to the northeast (until 40 km). This dispersion could have been associated to an unavoidable opening of the seismic network near the sea but most of the considered aftershocks have been re-located and show the same distribution (Yielding *et al.* 1989). In addition it could be attributed or correlated easily to the surface rupture features indicated by King & Yielding (1984) and linked to NW-dipping nodal planes with imbricated thrusting style as proposed by Yielding (1985). Ouyed *et al.* (1983) indicate that this could be due to the reactivation of a fan-like system of smaller reverse faults associated with surface folding. The depth distribution of the aftershocks is estimated between 2 and 10 km all along the rupture zone (Yielding *et al.* 1989). The mean depth of the fault planes is thereafter established around 6 km.

First, this aftershock distribution northwards allows us to propose a longer northeastern segment of about the same length than the two others (=12 km) and not simply 3–4 km as indicated by surface rupture features, leading to a total surface rupture length of 36 km. Then the aftershocks location between this northeastern segment and the sea, and their distribution in depth (King & Yielding 1984; Ouyed *et al.* 1983; Yielding *et al.* 1989), allow us to extend its width toward the north in our model, that is, closer to the sea. The proximity to the sea of the northeastern segment allows us to give more uncertainty for locating this one and to attribute to it realistic parameters.

As previously mentioned, the slip amplitude has been identified to be inconstant all along the rupture zone: all the studies conclude with a mean displacement (average value) of 3–4 m with maximum amplitude of about 6 m on the central segment (Cisternas *et al.* 1982;

Nabelek 1985; Yielding 1985). Constraining of the faulting mechanism with geodetic measurements of vertical movements (Cisternas *et al.* 1982; Ruegg *et al.* 1982; Bezzeghoud *et al.* 1995) a specific slip value has been determined for each segment of the rupture fault. These values are in good agreement with the relations between the observed mean surface displacement and the subsurface slip on the fault plane proposed by Wells & Coppersmith (1994): a magnitude  $M_w = 7.3$  earthquake leads to a ratio of 0.6–1.0 between the average subsurface displacement and the maximum surface displacement; thus a maximum surface displacement of 6 m corresponds to an average subsurface displacement on the fault plane of about 4–6 m. Our model fits as well as possible these previous results. This slip has been a bit exaggerated taking account of the other parameters. The related coseismic deformation is presented on Fig. 4.

All the corresponding parameters are summarized in Table 1.

### 2.3 Tsunami modelling

The initial bottom deformation is calculated based on elastic dislocation computed through Okada's formula (1985). Our method considers that the sea-bottom deformation is transmitted without losses to the entire water column, and solves the hydrodynamical equations of continuity (1) and motion (2) conservation. Non-linear terms are taken into account, and the resolution is carried out using a Crank Nicolson finite difference method centred in time and using an upwind scheme in space. This method has been widely used in the Pacific and Atlantic Oceans and the Mediterranean Sea and

contributes to tsunami hazard studies in several locations (Hébert *et al.* 2001; Roger & Hébert 2008; Sahal *et al.* 2009; Roger *et al.* 2010a,b):

$$\frac{\partial(\eta + h)}{\partial t} + \nabla \cdot [v(\eta + h)] = 0 \tag{1}$$

$$\frac{\partial v}{\partial t} + (v \cdot \nabla) \cdot v = -g\nabla\eta + \sum f \tag{2}$$

The wave propagation is calculated on the entire Alboran Sea and the area between the Spanish east coast and the Balearic Islands. A special focus on Alicante Harbour (0°29'W, 38°20'N) where the largest usable tsunami signal has been reported and registered in 1980 is also presented with the use of four levels of imbricated grids (from 0 to 3) of increasing resolution. The larger (first level, grid 0) is built from an interpolation of the Gebco World Bathymetric Grid 1' (IOC, IHO & BODC 2003) at a space step of 500 m. Then the grid resolution increases close to the studied site, that is, when the water depth *h* decreases along with the tsunami propagation celerity equation  $c = \sqrt{gh}$  which depends only on *h*, in the shallow water non-dispersive assumption.

Thus a high-resolution grid of Alicante Harbour, which is set up for the final grid level, is made from digitized, georeferenced and interpolated nautical bathymetric charts (SHOM 2001, 2005), in agreement with available harbour pictures, to complete the lack of bathymetric values near these structures. This grid has a resolution of 10 m (grid 3) and is able to reproduce the harbour major infrastructures such as docks or piers and coastal shallow water bathymetry (Fig. 3), which could have a significant influence on wave arrival times and amplitudes. Intermediate grids 1 and 2 are made with both datasets from grids 0 and 3. Grid 1 has been chosen to be at a 150 m resolution and grid 2 to be at a 50 m resolution in order to never have more than a factor of 4–5 between imbricated grids, in order to respect the Courant–Friedrichs–Lewy (CFL) criterion to ensure numerical stability (Courant *et al.* 1928) for each grid level, so that the shoaling effect is well reproduced and the wavelengths properly sampled. All these processes have been used in the case study of the Djijelli (Algeria) 1856 tsunami and its effects on the Balearic

Islands (Roger & Hébert 2008) and the Algerian coast (Yelles *et al.* 2009).

### 3 RESULTS

#### 3.1 Regional impact

First, the calculated initial deformation map presented in Figs 3 and 4 for both one- and three-segment sources shows that the initial coseismic deformation of an earthquake located at 45 km from the shore, with adequate parameters, is able to reach the sea. Thus the El Asnam earthquake itself could have been able to induce a small deformation of the sea surface and thus a tsunami. In fact, in each tested scenario, one of the major lobes of deformation (negative deformation) reaches the sea more or less and creates a deformation of the sea, that is, a tsunami, within a few centimetres (around 1–10 cm maximum; Figs 3 and 4).

Then this tsunami is able to propagate across the Mediterranean and the Alboran Sea.

It is worth noting that this coseismic deformation is able to induce submarine movements on the continental slope offshore Ténès as turbidity currents.

Fig. 5 represents the maximum wave heights reached at each point of the grids 0, 2 and 3 (Alicante Harbour) after 6 hr of tsunami propagation generated by the three-segment source scenario. We can see that some areas are more inclined to amplify the waves arriving from this part of the north African margin, offshore Ténès. The main sites showing noticeable amplification are, from the east to the west: the Spanish coast directly in front of the source area from the north east of Alicante to the neighbourhood of Cartagena (about 10 cm), including Alicante Harbour (40 cm) and the Balearic Islands; in fact the Balearic promontory seems to be particularly receptive to long wave amplification (as previously shown by Alasset *et al.* 2006; Roger & Hébert 2008; Sahal *et al.* 2009 in the case of the 1856 and 2003 northern Algeria events); the southern coasts of Ibiza and Formentera Islands (Fig. 5) show the most important wave heights about 15–20 cm (on this coarse grid 0; a better resolution would show most important wave heights in agreement with Green's Law (Synolakis 1991). Almeria Bay and the

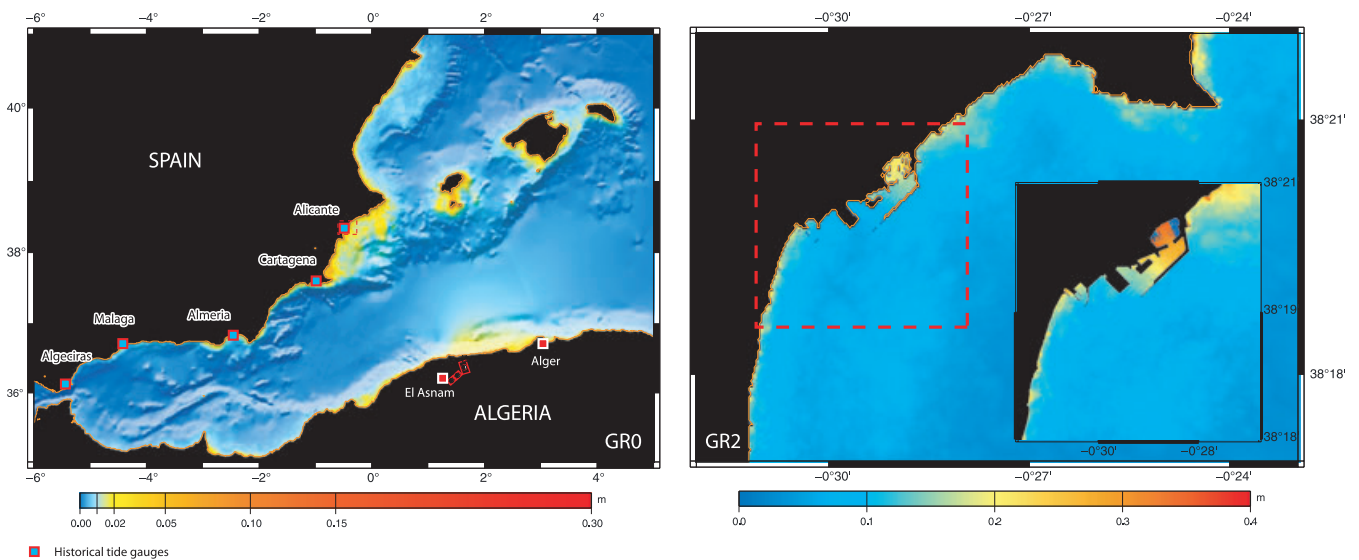


**Figure 5.** Maximum wave heights illuminated by bathymetric gradient on grid 0 (left-hand panel) after 6 h of tsunami propagation for a seismic source composed of three segments. Focus on Alicante Bay and Harbour are shown (right-hand panel). Historical tide gauge locations are also indicated (open red squares). Dashed boxes indicate the geographical location of GR2 and GR3, respectively.

neighbouring Malaga Bay (about 5–10 cm) are the most representative sites in the Alboran Sea.

The modelled maximum wave heights in coastal areas like Almeria or Malaga have been calculated on the 500 m resolution grid 0: this could result in a lack of coastal wave amplifications due to a shoaling effect or resonance phenomenon such as in Alicante Harbour. In fact we have not looked in detail into the other harbours where historical records have been found mainly because of the low tsunami amplitude (less than 10 cm) they show, which is hardly comparable to the modelling results.

The reader may notice that the wave heights in front of the peninsula northeast of Alicante could be related to submarine features such as canyons or low depths (as shown by Roger & Hébert 2008b in the case of the Minorca Canyon System in the Balearic Islands). Unfortunately, the lack of accurate bathymetric data in this area limits the use of modelling and thus does not allow us to conclude correctly.

In order to retrieve the tsunami waveform, a set of virtual tide gauges has been located everywhere on each grid. Some are located near the rupture area in order to control the initial sea surface deformation. Others are located in the maximum energy radiation zone (towards Alicante and the Balearic Islands) and in the Alboran Sea. We show the results of the two gauges of the Alicante inner and outer breakwater.

The two synthetic records in Alicante Harbour are shown on Fig. 6 concerning both the one- and three-segment rupture scenarios after 6 hr of tsunami propagation. The small initial coseismic deformation of about 10 cm offshore of Ténès (to the east, Fig. 4) has been able to induce sufficient sea surface deformation to propagate a tsunami towards the Spanish coast. The waves are composed of a first decrease of about 5 cm followed by an increase of about 5 cm of the sea level that is well reproduced by our model. The uncertainty in the arrival times indicated by Solovyev *et al.* (1992) allows us a range of possibilities for arrival times within several minutes. The period of the recorded signal is also well reproduced (around 15–20 min).

### 3.1.1 Note about arrival times in Alboran Sea (TTT)

The tsunami arrives in Malaga 1 hr 30 min after the seismic rupture and 2 hr in Algeciras (Fig. 1) which is in quite good agreement with the graphical estimation of arrival times from Solovyev *et al.* (1992) for Malaga, that is, more than 1 hr 10 min (Fig. 2). The 20 min difference could be related to wave slowing down when approaching the coast; due to the bad quality of bathymetric data along the coastline on this 500 m resolution grid, the synthetic gauge is not located at the exact location of the 1980 gauge, but farther from the coast, which could explain the 20 min delay. However there is a serious problem of arrival time for Algeciras that cannot be explained by the previous remark: in fact the amplitude of both signals is very small, about less than 1 cm peak to trough and maybe the tsunami arrival time has not been so well observed by Solovyev *et al.* (1991).

### 3.2 Impact in Alicante

The two historical records at Alicante Harbour are visible on Fig. 2. They are compared to the synthetic signals obtained with both scenarios (of one and three segments) in the harbour and outside (Fig. 6) corresponding to the outer and inner breakwater tide gauges indicated by Solovyev *et al.* (1992).

The only difference between the results of the simulations outside and inside the harbour concerns the tsunami amplitude showing a

factor 2 between the one-segment scenario and the three-segment scenario.

This tide gauge signals underlines the arrival times but also the wave main period and the amplitude reached. We can see that a free oscillation mode is well reproduced inside Alicante Harbour (Fig. 6, upper panel) about 2 hr after the first wave arrival inside the harbour and could be related to resonance phenomenon inside the harbour. On the outer gauge the oscillation period of about 12–15 min is particularly well reproduced on the first peaks for both scenarios, despite the lack of amplitude in the synthetic signal compared to the real signal (factor 1/3 for the three-segment scenario, 1/6 for the one-segment scenario).

## 4 DISCUSSION

### 4.1 The harbour responses

In both 1954 and 1980, the best signal and highest amplitude is recorded on the Alicante instruments. Without considering the particular hypothesis of a sufficient submarine landslide or a tsunami directly triggered by the earthquake, this is in agreement with the fact that Alicante is located in the direction perpendicular to the fault azimuth, that is, the major direction of deformation (Figs 3 and 4) and in the main tsunami propagation path according to Okal (1988).

In 1980, we can note that it is the inner breakwater mareogram that shows the highest historical amplitude of oscillations (peak to trough) of 48 cm whereas the outer record shows only a maximum amplitude of 15 cm (Solovyev *et al.* 1991). This amplification on the inner gauge is probably due to a resonant harbour effect that could be initialized by long wave arrival in a semi-enclosed water body. This occurs when the period of these waves is similar to the period of free oscillations (eigenperiod) of the water surface of the harbour (Bellotti 2007; Sahal *et al.* 2009).

Notice that the locations of our virtual tide gauges are adapted from the locations indicated by Solovyev *et al.* (1992). This could be responsible for substantial differences observed between recorded signals and synthetic ones especially on the outer gauge: first the water depth under the gauge must be considered and then the tide gauge (real or virtual) can be located at a node of oscillation or not (Wüest & Farmer 2003; Rabinovich 2009). In fact, concerning the inner gauge, the resonant effect could be better reproduced and prevails on the other phenomenon.

Finally, the shape of the harbour has changed in 30 years, according to actual satellite views compared with historical maps of the harbour; new docks and piers have been built and this has probably had some noticeable impact on the global eigenperiod of the harbour (Bellotti 2007; Gonzales-Marco *et al.* 2008).

### 4.2 A possible contribution by the turbidity currents: comparison with the 1979 Nice event

On 1979 October 16, a submarine landslide occurred close to Nice (southern France). The initial destabilization volume has been estimated to be about 10 million cubic metres which rapidly increased to reach a total amount of 150 million cubic metres with sediments stripped from the slope (Assier-Rzadkiewicz *et al.* 2000). This was probably the origin of an important turbidity current (Piper & Savoye 1993) that cut two submarine cables located, respectively, 75 and 105 km from the coast. Assier-Rzadkiewicz *et al.* (2000) indicate that the bathymetric data revealed the substantial

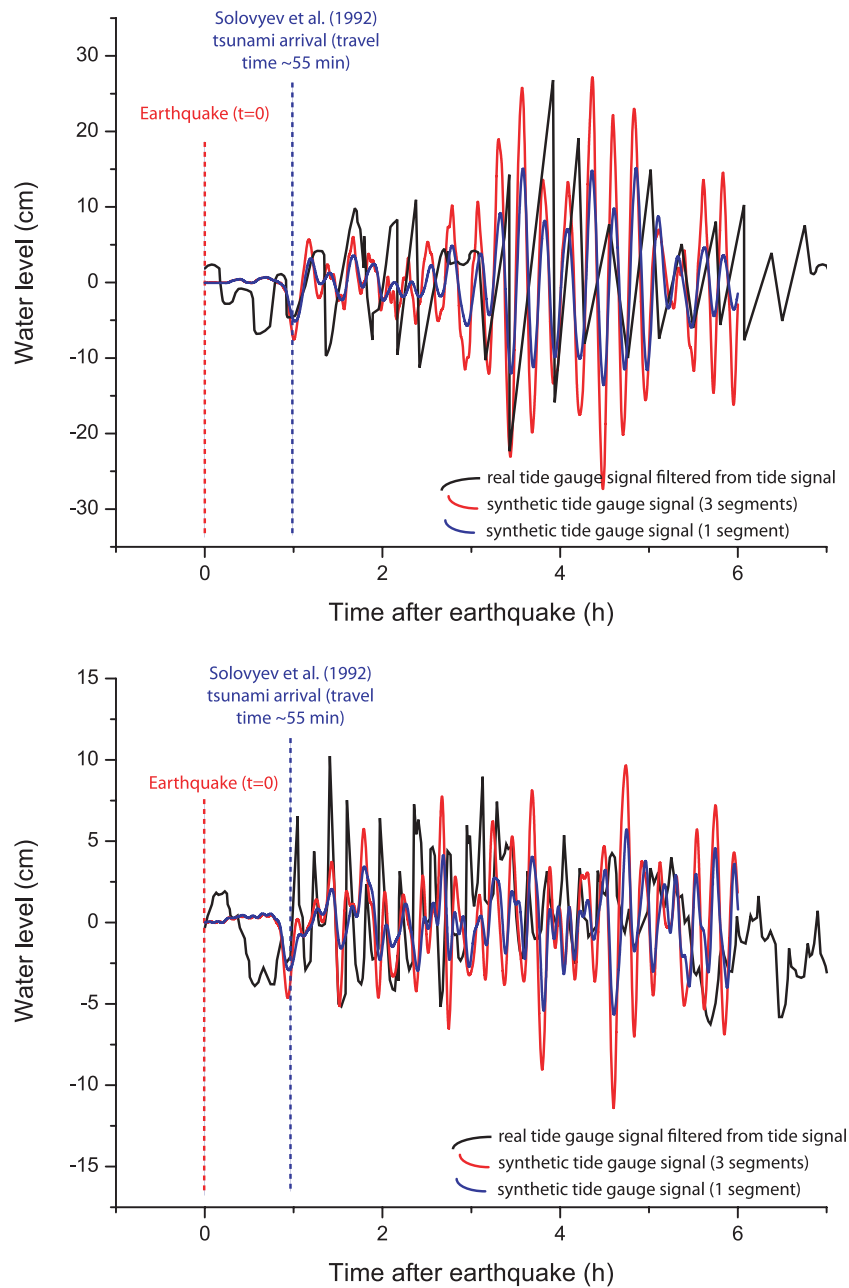


**Figure 6.** Synthetic signal registered on virtual tide gauges located in Alicante Harbour (see location of the gauges on Fig. 5 GR3): inner tide gauge (upper panel) and outer tide gauge (lower panel). The synthetic signal is superimposed on the real historical records (filtered from tide signal) at these two locations. Earthquake and tsunami times from Solovyev *et al.* (1992) are indicated.

modification of the sea-floor by this event and its path is indicated by a steeply incised chute.

A tsunami was induced by this submarine landslide with wave amplitude of about 3 m, 10 km away from the source at Antibes, in the Angel's Bay, and no more than a few dozen centimetres 30 km away (Mandelieu). This is due to the geometrical dispersion (frequency and amplitude dispersion) of waves on a sphere, explaining that the tsunami spectral amplitude decreases rapidly away from the source because of its multi-frequency composition typical of submarine landslide generated tsunamis (Okal 2003; Papadopoulos *et al.* 2007), and also because the observation site is not located within the main energy direction.

Assier-Rzadkiewicz *et al.* (2000) indicate that the period of each wave of the 1979 Nice event is estimated around 8 min, a value that

is probably related to the considered harbour resonance. According to the recent study of Ioualalen *et al.* (2010), the period of those waves in the source area has been estimated as about 2–3 min for this event.

## 5 CONCLUSION

This study proposes an alternative hypothesis for the tsunami generation during the 1980 October 10 event. It shows that tsunami-genic seismic sources don't have to be located at sea (as in Djijelli, 1856 August) or partially at sea (as in Zemmouri, 2003 May) to generate a small tsunami, and this without considering underwater landslide triggering tsunamis. In fact an inland earthquake located as far from the sea as the El Asnam earthquake of 1980

October 10 is able to generate a tsunami due to the repartition of initial rupture deformation lobes, according to numerical modelling. Indeed, the proposed parameters of the rupture scenarios, chosen with the help of previous geological and geodetic measurements, are able to explain the observed tsunami. The comparison of synthetic tide gauge records and historical records highlights that the observed wave periods are well reproduced: only a tsunami generated by an earthquake could show eigenperiod of 15–25 min, as the one shown by the different historical records, a typical period of a tsunami generated by a landslide hanging around several minutes (2–10 min).

In addition, either a simple segment rupture scenario or a three-segment scenario are able to reproduce correctly the historical signals in terms of wave arrival, polarity, amplitude and period. This is well shown on the records at Alicante Harbour. The main reason for using a multiple-segment source is to reduce the energy in the southwestern side of the rupture and to increase it on the opposite side, that is, near the shore. In general the traveltimes indicated by Solovyev *et al.* (1992) are in good agreement with modelled TTTs.

Nevertheless, such important earthquakes ( $M_w > 7.0$ ) could easily destabilize the unstable sediment cover along the margin and thus induce submarine mass movements and turbidity currents, which could also generate a local tsunami (one has been highlighted by a phone cable rupture in Algier's Bay on the same day). However several linked parameters should be considered in this case: the volume of the slide, the lack of wave observation along the Algerian coast, the period of the recorded signal along the Spanish southeastern coast and the dispersion phenomenon. A sediment movement able to produce a tsunami reaching Alicante and as far as Algeciras Harbour must be at least as important as the Nice 1979 event to produce a tsunami wave that would not disperse too fast. Bathymetric surveys offshore of the Algerian coast in this area have even not highlighted adequate scarps and no reports of huge coastal waves along the Algerian shore have been found.

The fact that the geodetic measurements led to a larger seismic moment value and that we use an artificial increase of seismic moment magnitude from 7.1 to 7.3 to reproduce the observations in terms of geodetic data but also tide gauge records allow us to indicate that tsunami data could help further investigation of seismic sources.

According to the modelling results and more particularly to the maximum wave height distribution maps, it could be interesting to investigate Ibiza and Formentera islands, which seem to be particularly inclined to wave amplification, in terms of harbour authority witnesses as well as on field proof, probably not for this recent event of 1980 but for potential older ones.

An accurate study of resonance phenomenon inside Alicante Harbour should be led in order to explain the origin of the 15–25 min oscillation period in 1980, using a coeval bathymetric map to produce the grid necessary for modelling. Then a comparison with the actual harbour shape could show whether the harbour still reacts or not to long wave arrival.

Tsunami modelling of the 1954 event could be done to show that this smaller rupture, in terms of energy, and in comparison to the 1980 event, is able to produce an even larger tsunami due to its geographical position closer to the shore (northeastward from the 1980 epicentre).

## ACKNOWLEDGMENTS

This research was funded by the European project TRANSFER (Tsunami Risk ANd Strategies For the European Region) under

the contract 0370 58, by the MAREMOTI project from the French ANR (Agence Nationale de la Recherche) under the contract ANR-08-RISKMAT-05-01c and by the LRC Yves Rocard (Laboratoire de Recherche Conventionné CEA-ENS). We are grateful to Eric Thauvin (CEA-DASE) for his precious help for bathymetric grids construction, Alain Rabaute (GeoSubSight company) and Pierpaolo Dubernet (ENS) for technical support, Carl Harbitz (Norwegian Geotechnical Institute) for constructive discussion about submarine landslides, Jocelyn Guilbert (CEA-DASE), Marc Nicolas (CEA-DASE), Mourad Bezzeghoud (Universidade de Evora), Raul Madariaga (ENS) and Paolo Marco De Martini (INGV) for constructive discussions about the earthquake of El Asnam in general and the source parameters. We would like to thank Wendy Austin-Giddings (BGS) for the proofreading of the manuscript and her interesting comments as well as the two anonymous referees.

## REFERENCES

- Alasset, P.-J., Hébert, H., Maouche, S., Calbini, V. & Meghraoui, M., 2006. The tsunami induced by the 2003 Zemmouri earthquake ( $M_w = 6.9$ , Algeria): modelling and results, *Geophys. J. Int.*, **166**, 213–226, doi:10.1111/j.1365-246X.2006.02912.x.
- Ambraseys, N.N., 1981. The El Asnam (Algeria) earthquake of 10 October 1980; conclusions drawn from a field study, Technical note. *Q. J. Eng. Geol. Lond.*, **14**, 143–148.
- Assier-Rzadkiewicz, S., Heinrich, P., Sabatier, P.C., Savoye, B. & Bourillet, J.F., 2000. Numerical Modelling of a Landslide-generated Tsunami: the 1979 nice event, *Pure appl. Geophys.*, **157**, 1707–1727.
- Bellotti, G., 2007. Transient response of harbours to long waves under resonance conditions, *Coastal Eng.*, **54**, 680–693.
- Bezzeghoud, M., Dimitrov, D., Ruegg, J.C. & Lammali, K., 1995. Faulting mechanism of the El Asnam (Algeria) 1954 and 1980 earthquakes from modelling of vertical movements, *Tectonophysics*, **249**(3–4), 249–266.
- Bilek, S.L. & Lay, T., 1999. Rigidity variations with depth along interpolate megathrust faults in subduction zones, *Nature*, **400**, 443–446.
- Boudiaf, A., Ritz, J.-F. & Philip, H., 1998. Drainage diversions as evidence of propagating active faults: example of the El Asnam and Thénia faults, Algeria, *Terra Nova*, **10**, 236–244.
- Bourcart, J. & Glangeaud, L., 1956. Perturbations sous-marines et courants de turbidité du séisme d'Orléansville, *CR Acad. Sci.*, **T242**, 1504–1506.
- Cattaneo, A. *et al.*, 2010. Submarine landslides along the Algerian Margin: a review of their occurrence and potential link with tectonic structures, in Submarine mass movements and their consequences, *Adv. Nat. Technol. Hazards Res.*, **28**, III, 515–525, doi:10.1007/978-90-481-3071-9\_42.
- Cisternas, A., Dorel, J. & Gaulon, R., 1982. Models of the complex source of the El Asnam earthquake, *Bull. seism. Soc. Am.*, **72**(6), 2245–2266.
- Courant, R., Friedrichs, K. & Lewy, H., 1928. Über die partiellen Differenzgleichungen der mathematischen Physik, *Mathematische Annalen*, **100**(1), 32–74.
- Deschamps, A., Gaudemer, Y. & Cisternas, A., 1982. The El Asnam, Algeria, earthquake of 10 October 1980: multiple-source mechanism determined from long-period records, *Bull. seism. Soc. Am.*, **72**(4), 1111–1128.
- Dewey, J.W., 1990. The 1954 and 1980 Algerian earthquakes: implications for the characteristic-displacement model of fault behaviour, *Bull. seism. Soc. Am.*, **81**(2), 446–467.
- Domzig, A., Gaullier, V., Giresse, P., Pauc, H., Deverchère, J. & Yelles, K., 2009. Deposition processes from echo-character mapping along the western Algerian margin (Oran-Tenes), Western Mediterranean, *Mar. Petrol. Geology*, **26**, 673–694.
- El-Robrini, M., Gennesseaux, M. & Mauffret, A., 1985. Consequences of the El-Asnam earthquakes: turbidity currents and slumps on the Algerian margin (Western Mediterranean), *Geo-Mar. Lett.*, **5**, 171–176.

- Geist, E.L. & Bilek, S.L., 2001. Effect of depth-dependent shear modulus on tsunami generation along subduction zones, *Geophys. Res. Lett.*, **28**(7), 1315–1318.
- Gonzales-Marco, D., Sierra, J.P., Fernandez de Ybarra, O. & Sanchez-Arcilla, A., 2008. Implications of long waves in harbor management: the Gijón port case study, *Ocean Coastal Manag.*, **51**, 180–201, doi:10.1016/j.ocecoaman.2007.04.001.
- Hanks, T.C. & Kanamori, H., 1979. A moment magnitude scale, *J. Geophys. Res.*, **84**(B5), 2348–2350.
- Harbitz, C.B., Lovholt, F., Pedersen, G. & Masson, D.G., 2006. Mechanisms of tsunami generation by submarine landslides: a short review, *Norwegian J. Geol.*, **86**, 255–264. ISSN 029–196X.
- Hébert, H., Heinrich P., Schindelé F. & Piatanesi A., 2001. Far-field simulation of tsunami propagation in the Pacific Ocean: impact on the Marquesas Islands (French Polynesia), *J. geophys. Res.*, **106**, 9161–9177.
- Heezen, B.C. & Ewing, M. (1955). Orléansville earthquake and turbidity currents, *Bull. Am. Assoc. Petrol. Geol.*, **39**(12), 2505–2514.
- IOC, IHO & BODC, 2003. Centenary Edition of the GEBCO Digital Atlas, British Oceanographic Data Centre, Liverpool, (CD-ROM).
- Ioualalen, M., Migeon, S. & Sardoux, O., 2010. Landslide tsunami vulnerability in the Ligurian Sea: case study of the 1979 October 16 Nice international airport submarine landslide and of identified geological mass failures, *Geophys. J. Int.*, **181**(2), 724–740.
- Kasser, M., Ruegg, J.C. & Lepine, J.C., 1987. Deformations associated with the El Asnam earthquake of October 10, 1980 (Algeria), in: Recent Movements in Africa, eds Wassef, A.M., Boud, A., Vyskocil, P., *J. Geodyn.*, **7**, 215–219.
- King, G. & Yielding, G., 1984. The evolution of a thrust fault system: processes of rupture initiation, propagation and termination in the 1980 El Asnam (Algeria) earthquake, *Geophys. J. R. astr. Soc.*, **77**, 915–933.
- King, G.C.P. & Vita-Finzi, C., 1981. Active folding in the Algerian earthquake of 10 October 1980, *Nature*, **292**, 22–26.
- Kulikov, E.A., Rabinovich, A.B., Thomson, R.E. & Bornhold, B.D., 1996. The landslide tsunami of November 3, 1994, Skagway Harbor, Alaska, *J. geophys. Res.*, **101**(C3), 6609–6615.
- Lammali, K., Bezzeghoud, M., Oussadou, F., Dimitrov, D. & Benhallou, H., 1997. Postseismic deformation at El Asnam (Algeria) in the seismotectonic context of northwestern Algeria, *Geophys. J. Int.*, **129**, 597–612.
- Nabelek, J., 1985. Geometry and mechanism of faulting of the 1980 El Asnam, Algeria, earthquake from inversion of teleseismic body waves and comparison with field observations, *J. geophys. Res.*, **90**(B14), 12 713–12 728.
- Okada, Y., 1985. Surface deformation due to shear and tensile faults in a half-space, *Bull. seism. Soc. Am.*, **75**, 1135–1154.
- Okal, E., 1988. Seismic parameters controlling far-field tsunami amplitudes: a review, *Nat. Hazards*, **1**, 67–96.
- Okal, E.A., 2003. Normal mode energetic for far-field tsunamis generated by dislocations and landslides, *Pure appl. Geophys.*, **160**(10–11), 2189–2221.
- Okal, E.A. & Synolakis, C.E., 2004. Source discriminants for near-field tsunamis, *Geophys. J. Int.*, **158**, 899–912.
- Ouyed, M. et al., 1981. Seismotectonics of the El Asnam earthquake, *Nature*, **292**, 26–31.
- Ouyed, M., Yielding, G., Hatzfeld, D. & King, G.C.P., 1983. An aftershock study of the El Asnam (Algeria) earthquake of 1980 October 10, *Geophys. J. R. astr. Soc.*, **73**, 605–639.
- Papadopoulos, G.A., Daskalaki, E. & Fokaefs, A., 2007. Tsunamis generated by coastal and submarine landslides in the Mediterranean Sea, Submarine Mass Movements and Their Consequences 3rd International Symposium, *Adv. Nat. Technol. Hazards Res.*, **27**, 415–422, doi:10.1007/978-1-4020-6512-5.
- Philip, H. & Meghraoui, M., 1983. Structural analysis and interpretation of the surface deformations of the El Asnam earthquake of October 10, 1980, *Tectonics*, **2**(1), 17–49.
- Piper, D.J.W. & Savoye, B., 1993. Process of late Quaternary turbidity current flow and deposition on the Var Deep-sea Fan, Northwest Mediterranean Sea, *Sedimentology*, **40**, 557–582.
- Rabinovich, A.B., 2009. Seiches and harbor oscillations, in: *Handbook of Coastal and Ocean Engineering*, pp. 193–236, eds Y.C. Kim, World Scientific Publ., Singapore.
- Roger, J. & Hébert, H., 2008a. Results of the modelling of the El Asnam (Algeria) earthquake of 1980, *Geophys. Res. Abst.*, **10**, EGU2008-A-02131.
- Roger, J. & Hébert, H., 2008b. The 1856 Djidjelli (Algeria) earthquake and tsunami: source parameters and implications for tsunami hazard in the Balearic Islands, *Nat. Hazards Earth Syst. Sci.*, **8**(4), 721–731.
- Roger, J., Hébert, H. & Briole, P., 2009. The tsunami triggered by the El Asnam (Algeria) earthquake of 1980: a new hypothesis of generation, *Am. Geophys. Un. Fall Meeting*, Abstract OS43A-1378.
- Roger, J., Baptista, M.A., Sahal, A., Allgeyer, S. & Hébert, H., 2010b. The transoceanic 1755 Lisbon tsunami in Martinique, *Pure appl. Geophys.*, in press, doi:10.1007/s00024-010-0216-8.
- Roger, J., Allgeyer, S., Hébert, H., Baptista, M.A., Loevenbruck, A. & Schindelé, F., 2010a. The 1755 Lisbon tsunami in Guadeloupe Archipelago: source sensitivity and investigation of resonance effects, *Open Oceanogr. J.*, **4**, 58–70.
- Rothé, J.P., 1955. Le tremblement de terre d'Orléansville et la sismicité de l'Algérie, *La Nature*, **3237**, 1–9.
- Ruegg, J.C., Kasser, M., Tarantola, A., Lepine, J.C. & Choukrat, B., 1982. Deformations associated with the El Asnam earthquake of 10 October 1980: geodetic determination of vertical and horizontal movements, *Bull. seism. Soc. Am.*, **72**(6), 2227–2244.
- Sahal, A., Roger, J., Allgeyer, S., Lemaire, B., Hébert, H., Schindelé, F. & Lavigne, F., 2009. The tsunami triggered by the 21 May 2003 Boumerdes-Zemmouri (Algeria) earthquake: field investigations on the French Mediterranean coast and tsunami modelling, *Nat. Hazards Earth Syst. Sci.*, **9**, 1823–1834.
- SHOM (Service Hydrographique et Océanographique de la Marine), 2001. Ports d'Alicante et de Torrevieja, 1/10000<sup>e</sup>. Publication 1969, 3rd edn, no. 6515.
- SHOM (Service Hydrographique et Océanographique de la Marine), 2005. Abords d'Alicante, 1/25000<sup>e</sup>. Publication 1991, 2nd edn, no. 7304 (INT 3167).
- Shah, H.C. & Bertero, V., 1980. El-Asnam earthquake, Algeria, 10th October 1980. Preliminary reconnaissance report. USGS reconnaissance activities report, 56 pp, <http://www.eeri.org/site/reconnaissance-activities/44-algeria/130-m73elasnam>.
- Solov'yev, S.L., Campos-Romero, M.L. & Plink, N.L., 1992. Orleansville tsunami of 1954 and El Asnam tsunami of 1980 in Alboran sea (Southwestern Mediterranean sea), *Izvestiya, Phys. Solid Earth*, **28**(9), 739–760.
- Stock, C. & Smith, E.G.C., 2000. Evidence for different scaling of earthquake source parameters for large earthquakes depending on faulting mechanism, *Geophys. J. Int.*, **143**, 157–162.
- Synolakis, C.E., 1991. Green's law and the evolution of solitary waves, *Phys. Fluids A*, **3**(3), 490–491.
- Tappin, D.R., Watts, P. & Grilli, S.T., 2008. The Papua New Guinea tsunami of 17 July 1998: anatomy of a catastrophic event, *Nat. Hazards Earth Syst. Sci.*, **8**, 243–266.
- Tappin, D.R., Watts, P., McMurtry, G.M., Lafoy, Y. & Matsumoto, T., 2001. The Sissano, Papua New Guinea tsunami of July 1998—offshore evidence on the source mechanism, *Mar. Geol.*, **175**, 1–23.
- Wells, D.L. & Coppersmith, K.J., 1994. New empirical relationships among magnitude, rupture length, rupture width, rupture area, and surface displacement, *Bull. seism. Soc. Am.*, **84**(4), 974–1002.
- Wüest, A. & Farmer, D.M., 2003. Seiches, in: *Encyclopedia of Science & Technology*, 9th edn, McGraw-Hill, New York, NY.
- Yelles Chaouche, K., 1991. Coastal Algerian earthquakes: a potential risk of tsunamis in Western Mediterranean? Preliminary investigation, *Sci. Tsunami Hazards, special issue*, **9**(1), 47–54.
- Yelles-Chaouche, A., Roger, J., Déverchère, J., Bracène, R., Domzig, A., Hébert, H. & Kherroubi, A., 2009. The 1856 tsunami of Djidjelli (Eastern Algeria): Seismotectonics, modelling and hazard implications for the Algerian coast, *Pure appl. Geophys.*, **166**, 283–300, doi:10.1007/s00024-008-0433-6.

- Yelles, K. *et al.*, 2009. Plio-Quaternary reactivation of the Neogene margin off NW Algiers, Algeria: the Khayr-Al-Din bank, *Tectonophysics*, **475**, 98–116, doi:10.1016/j.tecto.2008.11.030.
- Yielding, G., 1985. Control of rupture by fault geometry during the 1980 El Asnam (Algeria) earthquake, *Geophys. J. R. astr. Soc.*, **81**, 641–670.
- Yielding, G., Jackson, J.A., King, G.C.P., Sinval, H., Vita-Finzi, C. &

- Wood, R.M., 1981. Relations between surface deformation, fault geometry, seismicity, and rupture characteristics during the El Asnam (Algeria) earthquake of 10 October 1980, *Earth planet. Sci. Lett.*, **56**, 287–304.
- Yielding, G., Ouyed, M., King, G.C.P. & Hatzfeld, D., 1989. Active tectonics of the Algerian Atlas Mountains—evidence from aftershocks of the 1980 El Asnam earthquake, *Geophys. J. Int.*, **99**, 761–788.